Acta Crystallographica Section D
Biological Crystallography
ISSN 0907-4449

Patterson-guided *ab initio* analysis of structures with helical symmetry

Jiro Kondo,[a] Ludmila Urzhumtseva[a] and Alexandre Urzhumtsev[b,c]*

[a]Architecture et Réactivité de l'ARN, Université Louis Pasteur, Institut de Biologie Moléculaire et Cellulaire, CNRS, 15 Rue René Descartes, 67084 Strasbourg, France, [b]Institut de Génétique et de Biologie Moléculaire et Cellulaire, Département de Biologie et de Génomique Structurales, CNRS–ULP–INSERM, 1 Rue Laurent Fries, 67404 Illkirch, France, and [c]Physics Department, Nancy University, 54506 Vandoeuvre-lès-Nancy, France

Correspondence e-mail: sacha@igbmc.u-strasbg.fr

Received 6 May 2008
Accepted 12 August 2008

Patterson maps, which have a peak for intermolecular vectors between two molecules linked by a pseudo-translation, are widely used for structure solution. However, these maps may contain other peaks that indicate additional important information. In particular, if a molecule has internal symmetry, the Patterson maps may have a peak even when the relation between two molecules is other than a pure translation. A special and frequent case is a crystal that consists of molecules with pseudo-helical symmetry, like RNA or DNA, packed more or less parallel to each other. For such pairs of molecules, the Patterson peak does not simply link the molecular centres but is shifted along the helical axis. The shift is proportional to the rotation between the two molecules. The known step of the helix may be sufficient to obtain a system of linear equations whose solution gives an approximate position for the molecule. This technique may provide crucial information when molecular replacement fails to find a solution or suggests a number of candidates. Instead of repeating numerous molecular-replacement trials varying the model, a model may be positioned directly in place and be modified and refined directly. This Patterson-based search for molecular position has been tested with several solved crystals and has assisted in structure solution of RNA duplexes containing *Homo sapiens* cytoplasmic or mitochondrial ribosomal decoding sites (A sites).

1. Introduction

The molecular-replacement technique (for a review, see Rossmann & Arnold, 2001) is an appropriate tool to solve RNA and DNA structures. Many of these molecules have relatively well conserved structures possessing pseudo-helical symmetry. In practice, this helical symmetry complicates the identification of the correct solution among a number of variants. Also, experience shows that molecular-replacement searches are very sensitive to minor differences between the search model and the structure under question. The solution of difficult cases may be aided by the possibility of identifying the approximate molecular position without using the search model, by simply using the general features of the experimental data, and from being able to 'fix it by thinking' (Feynman & Leighton, 1985).

Crystallographic theory states that the Patterson map (Patterson, 1934, 1935), calculated as the Fourier series with unphased intensities of structure factors, is the autocorrelation function of the electron-density distribution. In particular, it has peaks in the interatomic positions when individual atoms are resolved. In macromolecular crystallography, the resolu-

tion is low, the number of atoms is large and their displacement parameters are relatively high, blurring these peaks.

Generally speaking, the Patterson maps do not show a peak for two macromolecules in the crystal unless their electron densities are similar. In particular, when a whole crystal structure or its large substructure has translational or pseudo-translation symmetry, the density in two large volumes of the unit cell becomes similar; the density autocorrelation for a given translation is increased and the corresponding peak in the Patterson map is amplified accordingly and becomes visible. Similarly, for a model with internal symmetry, some rotations allow the model to be superimposed onto its rotated copy. An easy artificial example is a model with cylindrical symmetry rotated around its axis.

Another example is an infinite helix with a step H. Let us suppose that this helix is centred at the origin and its axis coincides with the direction **Oz**. Let $\mathbf{u_z}$ be the unitary vector in this direction. The helical symmetry means that the helix is conserved after the transformation

$$\mathbf{r} \rightarrow \mathbf{r}_{\theta H} = R_{\mathbf{z}}(\theta)\mathbf{r} + (\theta H/2\pi)\mathbf{u}_{\mathbf{z}}, \quad (1)$$

where $R_{\mathbf{z}}(\theta)$ represents the rotation around the axis **Oz** by angle θ expressed in radians. Let us now consider the transformation

$$\mathbf{r} \rightarrow \mathbf{r}_{\theta \mathbf{t}} = R_{\mathbf{z}}(\theta)\mathbf{r} + \mathbf{t}, \quad (2)$$

where $\mathbf{t}$ is a translation vector. Of course, the initial helix does not coincide with the transformed one if we simply translate it by the vector $\mathbf{t}$. However, it coincides if we translate it by

$$\mathbf{t}' = \mathbf{t} - (\theta H/2\pi)\mathbf{u}_{\mathbf{z}}. \quad (3)$$

As a consequence, the Patterson map should have a peak at $\mathbf{t}'$. A practical example is a model consisting of many nucleic acids. Fig. 1(*a*) shows a superposition of two copies of a 16-mer RNA duplex (Pan *et al.*, 1998) linked by a pure rotation of 120° (one third of a full turn) around the helical axis; their separated images are given on the left. Obviously, the initial model does not coincide with the rotated one centred at the origin. However, a translation of the initial model down by approximately 10 Å (one third of the step H of the RNA helix, which is approximately 30 Å) superimposes a major portion of the models well. The density correlation is not perfect at the atomic level but seems to be high when working at a resolution near 3–5 Å (see §3 for a more detailed study), which is usually the case for molecular replacement. If such a correlation is significant enough to give a peak in the Patterson map, it could be used as an additional tool to solve some difficult cases, since it does not require a search model. In particular, this could be important in molecular replacement when the search model is quite poor, the translation function does not give a signal and only the experimental information (a set of $F^{\rm obs}$) can be used.

An important observation is that for this crystal the direction of the molecular helical axis can be determined directly from the experimental structure-factor intensities (see §3). This is more generally true for many crystals of such elongated molecules with pseudo-helical symmetry. Firstly, the cross-rotation function, even with a poor model, indicates the direction of the molecule more or less correctly while having difficulty in giving the correct orientation around this helical axis (see, for example, Ogihara *et al.*, 1997). Secondly, this direction is also often directly detectable from the Patterson maps as shown below (§2.2).

Owing to their specific shape and interatomic interactions, these molecules are often packed roughly parallel to each other. Therefore, when the crystal contains several copies of the molecule with roughly parallel helical axes, the direction of these axes can be estimated and analysis of the Patterson peaks may help in structure solution.

It may be noted that a detailed analysis of three-dimensional Patterson maps has previously been used intensively, particularly in the very first studies of DNA (Franklin & Gosling, 1955), RNA (Kim & Rich, 1969; Sakurai *et al.*, 1971) and protein structures (Magdoff *et al.*, 1956). This manuscript discusses the use of the Patterson function, namely the detail of its central peak and the positions of off-origin peaks, in the molecular-replacement solution of difficult structures. For RNA duplexes containing the *Homo sapiens* cytoplasmic or mitochondrial ribosomal decoding sites (A sites), crystals of different crystal forms were available and for practically all of them structure determination with molecular replacement was not straightforward. Some of these structures were used as test cases and others were solved using the technique as described in the article.

In the following, the letters u, v and w represent the coordinates of the Patterson peaks and the letters x, y and z represent molecular crystallographic coordinates.

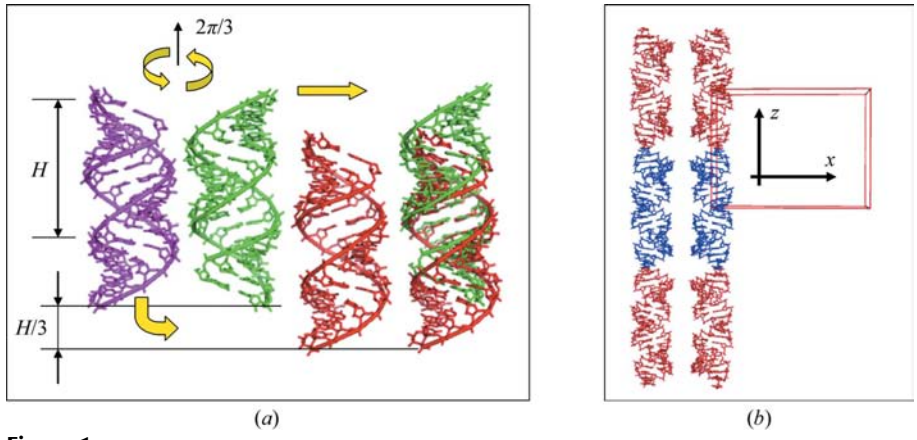

Figure 1
(*a*) Superposition of RNA models (16-mer RNA duplex; Pan *et al.*, 1998). The initial model is shown in magenta, the model rotated by 120° around its helical axis is shown in green, the initial model shifted by $-H/3$ along the helical axis is shown in red and a superposition of rotated and shifted models is shown on the right. (*b*) The artificial 23-mer RNA duplex used in tests with simulated data.

The programs *GLRF* (Tong & Rossmann, 1990; 1997), *FFTCAN* (Vernoslova & Lunin, 1993), *SF2CNS* (Urzhumtsev & Urzhumtseva, 2002), *PyMOL* (DeLano, 2002), *CONVROT* (Urzhumtseva & Urzhumtsev, 1997) and *CRYC3D* (Urzhumtseva & Urzhumtsev, 2008) were used to calculate rotation-function and Patterson maps, to visualize them and to analyze the geometry.

2. Patterson function with the simulated data

2.1. Intermolecular off-origin peaks in the Patterson maps

To study the features of off-origin peaks in Patterson maps, a 23-mer RNA-duplex model with standard geometry was generated [this model was used for molecular-replacement searches for RNA duplexes containing the *H. sapiens* cytoplasmic or mitochondrial ribosomal decoding site (A site) described below]. The length of the molecule is about 57 Å and the diameter of the helix is ∼20 Å. This model was oriented along **Oz** and packed at the centre of the orthogonal unit cell with dimensions 80, 40 and 60 Å (Fig. 1*b*). Space group *P*1 was taken. A second copy of the same molecule was positioned shifted by 30 Å along *x*. This second model either had the same orientation (pure translation) or was rotated by a given angle (30, 60, 90, 120, 150, 180°) around **Oz**. For each pair of models, structure factors were calculated and Patterson syntheses were obtained with corresponding magnitudes. The resolution of the syntheses varied from 2 to 9 Å.

In these maps (Fig. 2*a*) the height of the peak at the origin was several tens of σ and its features are discussed below in §2.3. At lower but still statistically significant cutoff levels varying from 2σ to 6σ each of these maps contained an off-origin peak at the distance of 30 Å in the *u* direction. When the rotation angle between the models was varied from 0 to 180°, the peak moved in the *w* direction by a distance that varied from 0 to approximately 15 Å in complete agreement with (3). The size of the peak decreased smoothly with rotation (Fig. 2*b*). This can be explained by an imperfection of the symmetry and some deviation of the rotation axis from **Oz** and also by the fact that the superimposed part of the models becomes smaller for larger rotations.

When the helical axis of the molecule is not fully aligned with the rotation axis, the superposition of the initial and rotated models after optimal translation is poorer. The larger

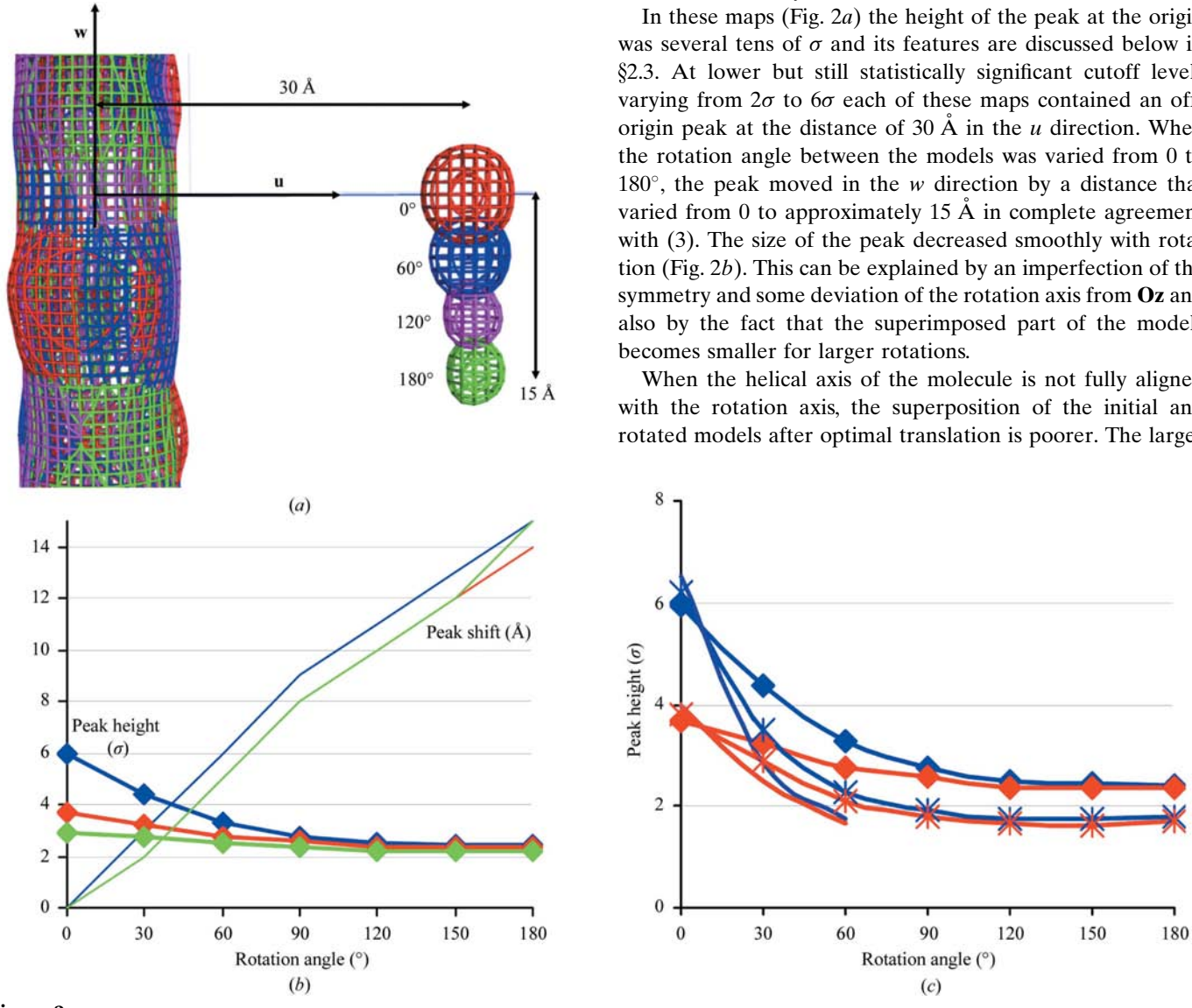

Figure 2
Patterson maps for simulated data. (*a*) Superimposed maps at 6 Å resolution and 2σ cutoff level. Different colours correspond to different rotation angles relating the two models as indicated. The origin peak at such a low cutoff level is seen as a continuous tube along **Ow**. The off-origin peak decreases and shifts downwards according to the rotation angle. (*b*) Peak height (lines with markers) and shift in the **w** direction (no markers) of the off-origin peak in the Patterson maps at 3 Å (blue), 6 Å (red) or 9 Å (green) resolution as a function of the rotation angle between the two models; the helical axis is parallel to the rotation axis **Oz**. (*c*) Peak height of the off-origin peaks in the Patterson maps at 3 Å (blue) or 6 Å (red) resolution as a function of the rotation angle between the two models; the helical axis makes an angle of 0° (rhombs), 10° (stars) or 20° (no markers) with the rotation axis **Oz**. For the model inclined by 20° and for rotations larger than 60°, the peaks are lower than other (noise) peaks in the maps and are not shown as curves.

the angle between these two directions, the poorer the superposition and the smaller the peak in the Patterson function (Fig. 2*c*). Nevertheless, when the angle between the helical and rotation axes is below 10°, the characteristics of the peak are similar to the ideal case of parallel axes. When this difference in axes approaches 20°, for rotation by small angles (30–50°) the peak is still the largest one. However, for larger rotation angles it becomes smaller than other peaks (some of these relatively weak peaks may correspond to other structural details or computation effects) and can no longer be used to identify necessary structural information. This loss of information is illustrated in Fig. 2(*c*) by the abruption of the corresponding curves at 60°.

2.2. Off-origin peaks in Patterson maps for a single molecule

The Patterson peak at the origin is highly anisotropic for pseudo-helical molecules (Fig. 2*a*) owing to this symmetry and reflects a high model coincidence with the original molecule when moving the model along its helical axis for a certain distance. This feature can be used to indicate the direction of the helical axis without running the cross-rotation function and, generally speaking, without any model.

A new simulated data set has been prepared in which only a single molecule at the origin of the unit cell has been left in the model crystal, similar to the previous tests. Of course, the details of the peak strongly depend on the resolution used. First of all, when all low-resolution data are included, the origin peak is always observed as a connected blob. At all resolutions, the maps show the next strongest peak at a distance of approximately 30 Å on **Ow** (Fig. 3), corresponding to the periodicity of the structure. Naturally, this peak is very strong for the particular example where the molecules form quasi-continuous packing; for a shorter molecule this peak may be much weaker or even absent. Also, this peak is smaller when low-resolution data (for example, all reflections with the resolution lower than 10 Å) are removed from the synthesis calculation, showing that the helical symmetry is only approximate.

There is a smaller peak at a distance of approximately 15 Å (Fig. 3) along **Ow**. This peak may correspond to the shift between the two RNA chains. To confirm this hypothesis, a similar Patterson map has been calculated for the model where one of the chains has been removed. In this map, this peak is clearly absent. In practice, the distance from this peak to the origin may vary slightly depending on the conformation of a particular molecule.

2.3. Asymmetry of the origin peaks in the Patterson maps

The central peak of the Patterson map for helical models also shows some features. First of all, for all resolutions verified between 2 and 9 Å the peak is elongated in the direction of the helical axis. Naturally, this anisotropy is less pronounced when the resolution is lower. When increasing the resolution and density-cutoff level (Fig. 3), the ellipsoid becomes a sphere with two blobs at its ends in the direction of the helical axis.

When low-resolution data (for example lower than 15 or 10 Å) are excluded, these features are conserved in maps at 4 Å resolution and lower. However, in maps at 2 or 3 Å resolution the blobs at the extremities of the central peak separate. The position of their centre relative to the origin does not depend on the resolution (2 or 3 Å), proving that they are not caused by Fourier series truncation but appear owing to structural features. Their distance of approximately 3.5 Å leads one to believe that these peaks correspond to a possible superposition of electron density for base pairs. Naturally, there is no atom-to-atom correspondence but a partial overlap of the density for a shift of approximately 3.4–3.5 Å in the direction of the helical axis. To check this hypothesis, a new simulated data set was obtained from the model in which each second base pair was removed. In the new maps, these peaks disappeared.

In summary, the features of the Patterson peaks discussed in §§2.2 and 2.3 may help to identify the orientation of an elongated model with helical pseudo-symmetry as is the case for many RNA and DNA molecular crystals. Naturally, these peaks may be merged, deformed or even disappear when the crystal contains molecules in different orientations or when the resolution varies. §2.1 gives an idea of how the off-origin peaks in the Patterson maps could provide information on the

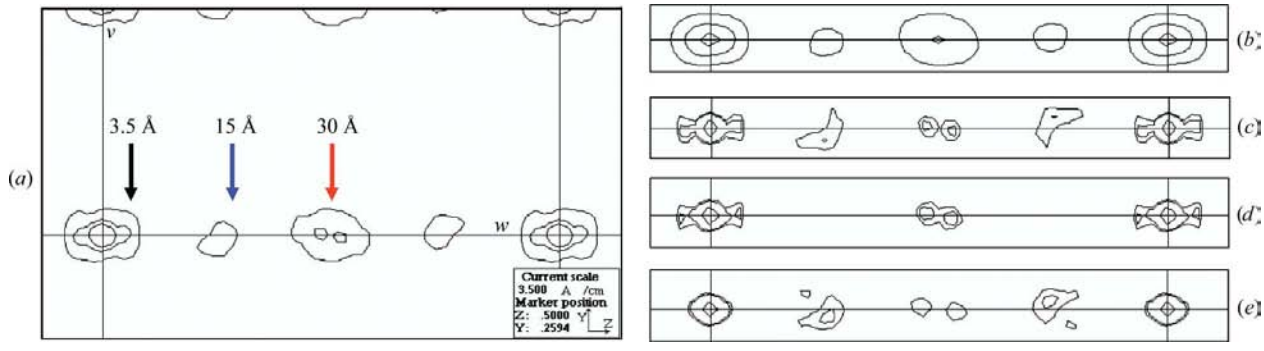

Figure 3
Patterson maps for simulated data, section *vOw*, $u = 0$. Cutoff levels are 4σ, 6σ and 8σ in (*a*) and (*b*) and 5σ, 10σ and 50σ in the other maps. For (*b*)–(*e*), only the region around **Ow** (horizontal) is shown. Coloured arrows indicate the specified distances along the helical axis aligned with **Ow**. (*a*) Resolution 3–100 Å; (*b*) resolution 6–100 Å; (*c*) resolution 3–10 Å, satellites of the central peak are clearly seen; (*d*) resolution 3–10 Å, one chain removed, peak at 15 Å has disappeared; (*e*) resolution 3–10 Å, each second base pair removed, satellites at 3.5 Å have disappeared.

relative position of molecules in the unit cell for a particular packing often observed for nucleic acids, as shown below.

3. Patterson analysis of the 16-mer RNA duplex

The structure of the 16-mer RNA duplex r(GCAGACUUAAAUCUGC)$_2$ (Pan *et al.*, 1998; PDB code 405d) crystallized in the rhombohedral system has been reported in a centred hexagonal cell with one duplex per asymmetric unit. The unit-cell parameters are $a = b = 42.56$, $c = 124.05$ Å. In this space group, $H3$, the choice of the origin following the **Oz** axis is arbitrary. Therefore, the centre of one of the models may be chosen at $z = 0$. All the computations below were performed with the experimental structure-factor magnitudes.

The molecule has internal noncrystallographic twofold rotation symmetry with an axis normal to the helical axis. The self-rotation function, which does not require any model to be calculated, clearly shows that the direction of this axis (Fig. 4*a*) coincides with **Ox**.

The Patterson maps at 3 and 6 Å resolution (Figs. 5*a* and 5*b*) showed a number of peaks along **Ow** (at distances of 3.5, 13 and 30 Å) in agreement with the theory in §§2.2 and 2.3, thus indicating **Oz** as the direction of the helical axis. The last key parameter required to position a model was therefore the crystallographic coordinates $(x, y, 0)$ of the molecular centre in the plane xOy.

Rotation of the model around **Oz** by 120° (the symmetry operation of the space group) is described by the transformation of the crystallographic coordinates

$$(x, y, z) \rightarrow (-y, x - y, z). \quad (4)$$

According to (1)–(3), for a structure with a period of about 30 Å aligned with the rotation axis, the peak in the Patterson map for the model rotated by $\theta = 120°$ should have an additional shift

$$\Delta_z = -\theta H/2\pi = -H/3 \simeq -10 \text{ Å} \quad (5)$$

along the rotation axis. Therefore, it follows from (4) and (5) that the Patterson peak should have crystallographic coordinates

$$(-x - y, x - 2y, -\Delta_z/c). \quad (6)$$

Indeed, the section $n_w = -10/120$, where $N_w = 120$ is the number of grid points on w (Fig. 5*d*), contained a very strong peak. In the 3 Å resolution map, this Patterson peak with coordinates $u = 0.18$ and $v = 0.59$ was the strongest peak, with the obvious exception of the peaks arising from the centred cell. Naturally, u and v may be increased by any integer, thus giving the coordinates of the equivalent peaks arising from unit-cell translations. In particular for $u = -0.82$ and $v = -0.41$ the solution of the system of equations

$$\begin{cases} -x - y = u = -0.82 \\ x - 2y = v = -0.41 \end{cases} \quad (7)$$

gave the solution $x \simeq 0.41$, $y \simeq 0.41$. The choice of the z coordinate was arbitrary.

Indeed, the coordinates of the centre of the model taken from the PDB are (0.42, 0.42, 0.04). This excellent coincidence illustrates how this structure could be solved 'on paper' using the Patterson functions.

Other values of u and v on the right side of (7) give either equivalent solutions outside the ranges $0 \leq x < 1$ and $0 \leq y < 1$ or for $u = -0.82$ and $v = 0.59$ a solution inside this range but corresponding to an alternative choice of unit-cell origin.

Section $n_w = -10/120$ contained two other peaks linked to the analyzed peak by crystallographic symmetry (Fig. 5*d*). A

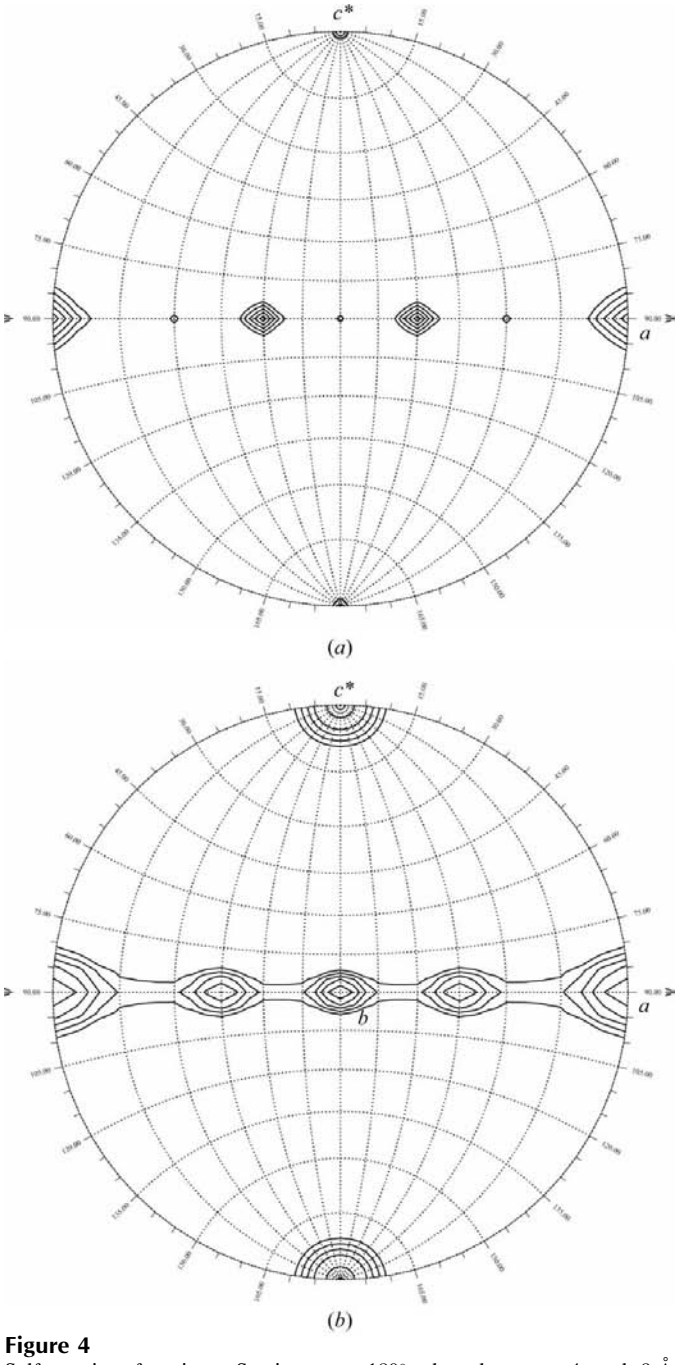

Figure 4
Self-rotation functions. Section $\kappa = 180°$; data between 4 and 9 Å resolution were used; the integration radius was 15 Å. (*a*) 16-mer RNA (PDB code 405d); (*b*) *H. sapiens* cytoplasmic A site, orthorhombic form.

choice of their coordinates as (u, v) would give the positions of the symmetry-related model with the internal dyad along **Oy** or $-$**Ox** $-$ **Oy**, respectively. It was not known *a priori* which Patterson peak corresponded to which model orientation. Therefore, when solving an unknown structure all possible combinations of model positions and orientations should be tried. Two strategies may be envisaged. When the model orientation is fixed (*e.g.* the molecular internal dyad is along the **Ox** axis), all three Patterson peaks should be tried in order to choose the one corresponding to this orientation. Alter-

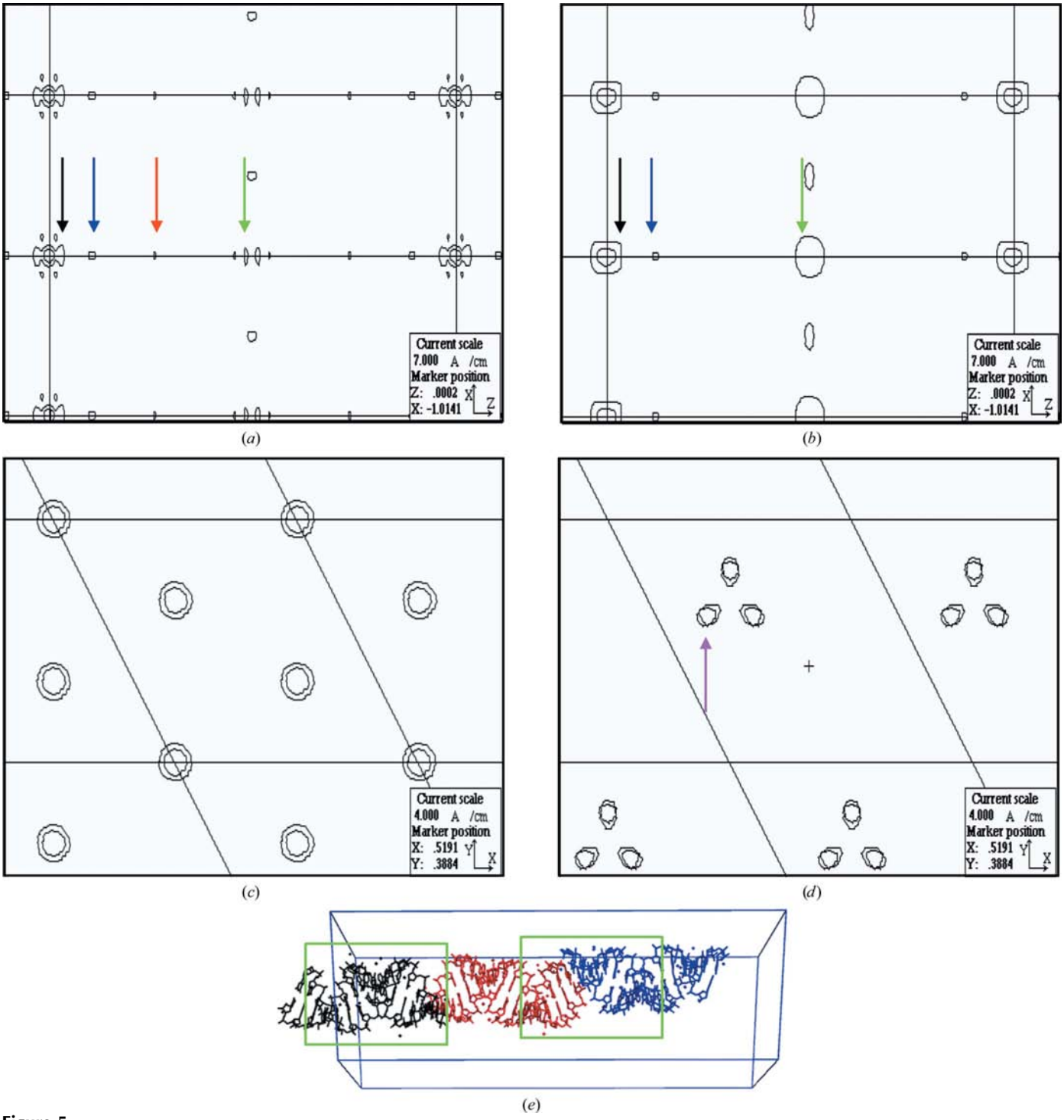

Figure 5
Patterson function for 405d. (*a*, *c*, *d*) Maps at 3 Å resolution with cutoff levels 3σ and 15σ and (*b*) at 6 Å resolution with cutoff levels of 2σ and 10σ. (*a*, *b*) Section $v = 0$; peaks at distances of 3.5, 13, 30 and 60 Å along the w axis are indicated by coloured arrows. (*c*) Sections $w = 0$, 40 and 80 ($N_w = 120$) superimposed showing the peaks for the molecules linked by translations arising from the centred unit cell. (*d*) Section $w = -10$ showing the Patterson peaks (two maps superimposed) for the molecules linked by a threefold axis. (*e*) Packing of the molecules in columns on z showing pseudo-translation by approximately 60 Å (green frames).

natively, a Patterson peak may be fixed and the model checked in each of three possible orientations.

In the 6 Å resolution map the Patterson peak was also very strong and could be used in the considerations above, giving the same results. However, at this resolution it is not the strongest peak. There is one stronger peak at $(0, 0, \frac{1}{2})$, *i.e.* at a distance of 60 Å along the **Oz** axis (Fig. 5*b*). This peak can be explained by approximate periodicity of the molecular 'columns' along **Oz** (Fig. 5*e*); this periodicity became more clear at lower resolution when losing atomic detail.

The crystal of the RNA duplex 405d showed that the Patterson function (including self-rotation function) and knowledge of the helical character of the molecule could quite unambiguously give its orientation and position in the cell without running a molecular-replacement search and, most importantly, in the absence of a highly similar model.

4. Patterson analysis of the *H. sapiens* cytoplasmic A site, $P2_12_12$ crystal

RNA duplexes containing the *H. sapiens* cytoplasmic or mitochondrial A site have been crystallized in several crystal forms. For practically all of them, the standard molecular-replacement method had difficulty in finding the solution; special efforts were required that have been described elsewhere (Kondo *et al.*, 2006; Kondo & Westhof, 2008). This article shows an application of the current Patterson-based approach to some of these crystals.

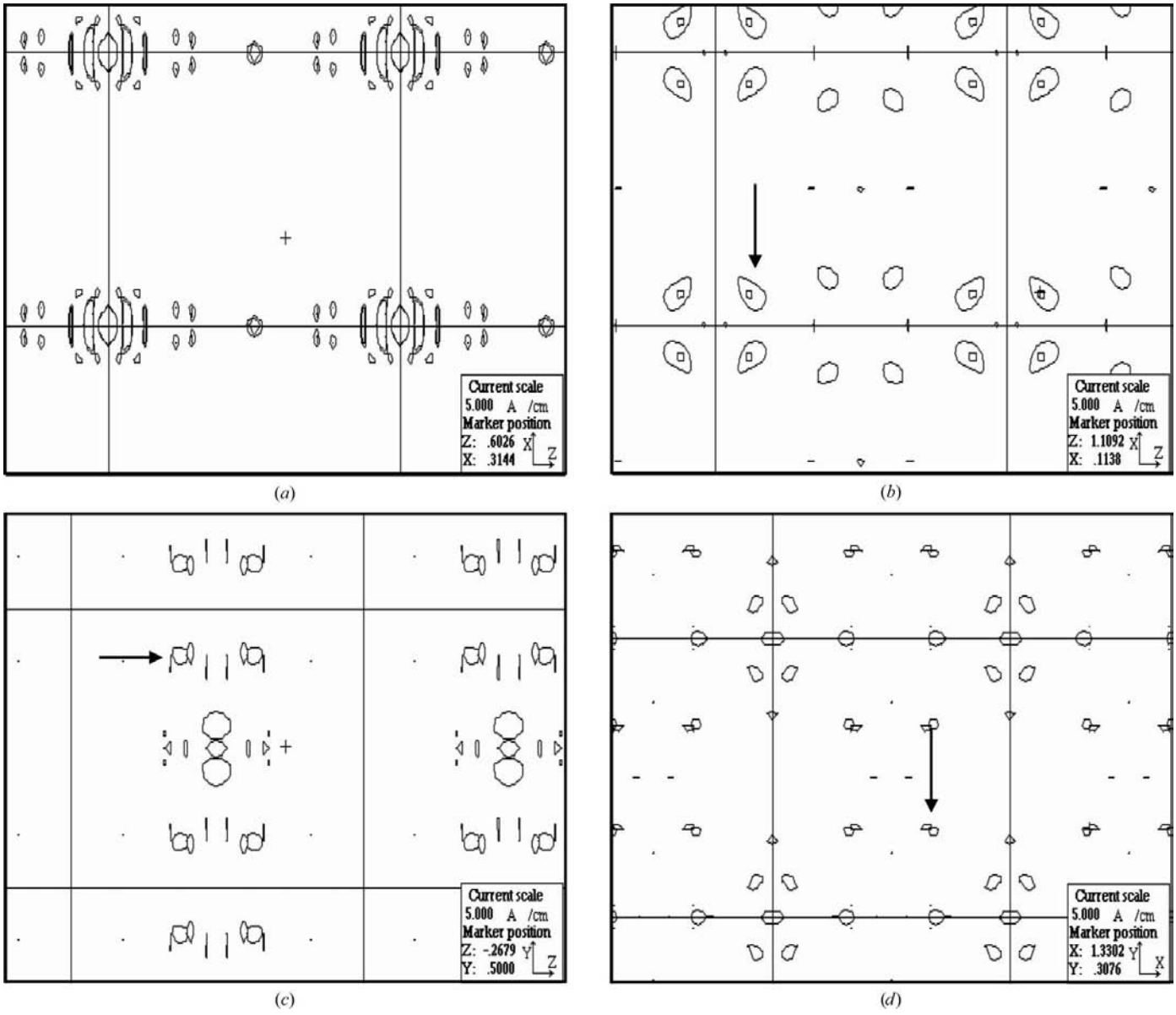

Figure 6
Patterson function for the *H. sapiens* cytoplasmic A site orthorhombic crystal. (*b*–*d*) show superposition of the maps at 3 and 6 Å resolution. For the superimposed maps, the common peaks are indicated by arrows. (*a*) Resolution 3 Å, cutoff 2σ and 3σ. Peaks along **Ow** are seen; a small deviation from **Ow** can be observed. (*b*) Harker section $v = \frac{1}{2}$, cutoffs 3σ (3 Å map) and 2σ (6 Å map). (*c*) Harker section $u = \frac{1}{2}$, cutoff 2σ for both maps. (*d*) Harker section $w = -\frac{1}{2}H/c$, cutoffs 1.5σ and 1.0σ, respectively.

One of the crystals belongs to space group $P2_12_12$, with unit-cell parameters a = 46.16, b = 47.06, c = 56.74 Å. The asymmetric unit contains one duplex with the dyad perpendicular to the helical axis (this information was known *a priori*). Both *AMoRe* (Navaza, 1994) and *Phaser* (McCoy *et al.*, 2005) gave the same position of the search model that could not be refined and was discovered (finally) to be incorrect. Further analysis allowed Kondo *et al.* (2006) to solve the structure and refine the model. This structure was used as a test case for the current approach.

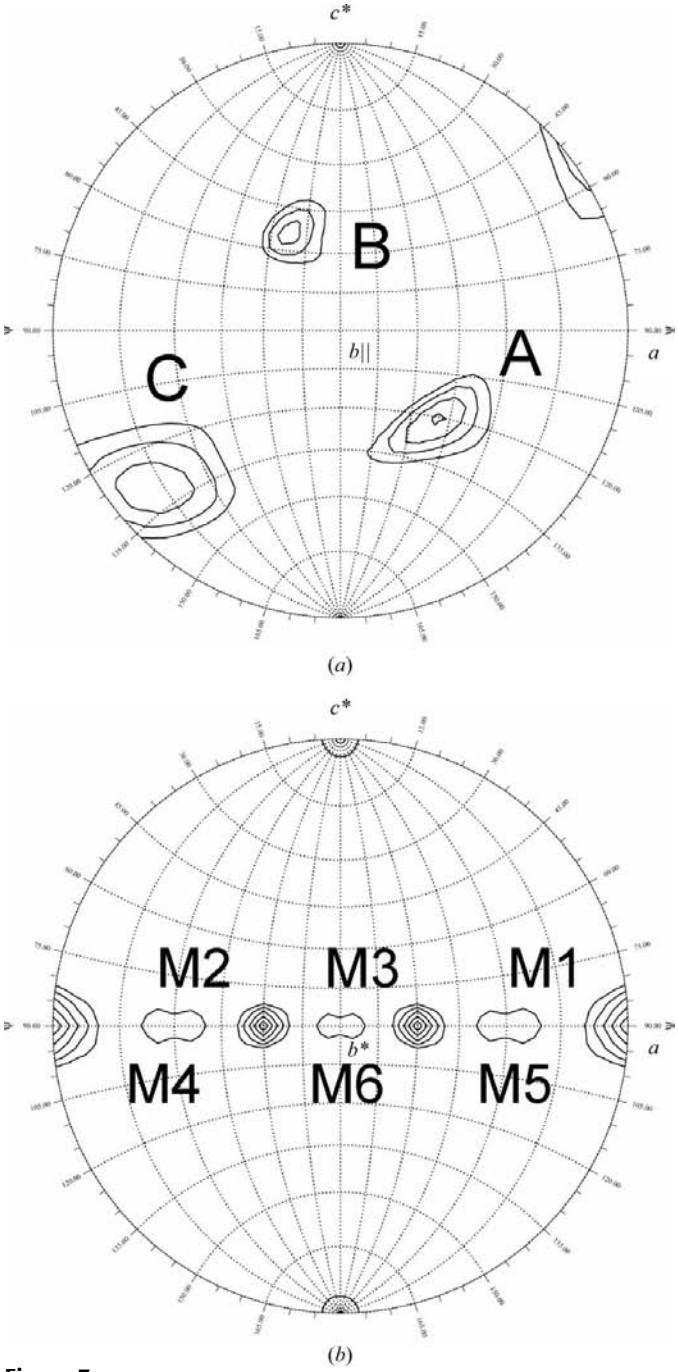

Figure 7
Self-rotation function for the *H. sapiens* mitochondrial A site. Section κ = 180°; data between 4 and 9 Å resolution were used; the integration radius was 10 Å. (*a*) Triclinic form: A, B and C indicate the directions of the dyads. (*b*) Trigonal form: M1–M6 indicate the directions of the internal dyad for the molecules as defined in the text.

By its anisotropy, the central peak of the Patterson maps at 3 Å resolution (Fig. 6*a*) indicated that the helical axis is practically parallel to the **Oz** axis; peaks may be found at distances of 3.5 and 14 Å as discussed in §§2.2 and 2.3. The self-rotation function (Fig. 4*b*) showed the direction of the internal dyad approximately following the diagonals $x = \pm y$, $z = 0$ (angle φ, the axis with **Ox**, is approximately ±45°). Table 1 shows the coordinates of the centres of the molecules and the expected Patterson peaks between them where (x, y, z) represents the position of molecule M1 with the dyad following $\varphi = 45°$. All these peaks belonged to Harker sections (Harker, 1936) where one coordinate was independent of the coordinates of the molecular centre: $u_{\rm Harker} = \frac{1}{2}$, $v_{\rm Harker} = \frac{1}{2}$ or $w_{\rm Harker} = \pm\frac{1}{2}H/c$. In the latter, c is the unit-cell parameter and H is the period of the helix, giving $w_{\rm Harker}$ = 0.26, or section n_w = 15/56 (grid numbers N_u = 48, N_v = 48, N_w = 56 were used in this test).

Indeed, the section n_v = 24/48, or Harker section $v_{\rm Harker} = \frac{1}{2}$, contained a clear peak at 2σ in maps at both 3 and 6 Å resolution corresponding to the transformation M1→M3 (Fig. 6*b*). Its coordinates (0.10, 0.11) gave the molecular centre at x = 0.20, z = 0.88. In the section n_u = 24/48, or Harker section $u_{\rm Harker} = \frac{1}{2}$, the only common peak in the two maps (Fig. 6*c*) had coordinates (0.82, 0.39) giving, from M1→M2, the coordinates of the molecular centre at y = 0.39, z = 0.87. Finally, the section $n_w = -15/56$, or $w_{\rm Harker} = -\frac{1}{2}H/c = -0.26$, also had a single common peak at both resolutions (Fig. 6*d*). However, this peak was weaker and was only seen at 1.0–1.5σ. This lower signal is in agreement with the theory as it corresponds to a larger rotation angle of 180° instead of 90° as for the two previous peaks. This peak can be used for checking but cannot be used as a sure source of information. The peak coordinates (0.65, 0.30) give the values x = 0.17, y = 0.35.

The final independently solved structure had coordinates of the centre of x = 0.20, y = 0.35, z = 0.88. Thus, the position found analytically corresponds well to the solution. For the wrong solution suggested by molecular replacement (see Kondo *et al.*, 2006), it was observed that the model was in the correct density but rotated around the helical axis and shifted along it accordingly. This wrong model had the dyad oriented at $\varphi = -45°$ and model refinement could not progress. The Patterson-based solution, if available at the time, could fix the problem immediately.

5. Structure solution of the *H. sapiens* mitochondrial A site, triclinic crystal

The approach described above was used in the structure solution of three more crystals of the *H. sapiens* mitochondrial A site. The first crystal belongs to space group *P*1, with unit-cell parameters a = 35.14, b = 45.46, c = 52.13 Å, α = 71.43, β = 73.42, γ = 74.05°. Its asymmetric unit cell contains two identical duplexes, each with internal twofold pseudosymmetry. The molecule was expected to be helical with a length of approximately 55 Å. Various molecular-replacement pro-

Table 1
Transformations and the equivalent directions corresponding to the internal molecular dyad.

The molecular dyad is always in the plane *xOy*. *c* is the corresponding unit-cell parameter and $H_c = H/c$ is the molecular period in fractional coordinates following **Oz**. 'Angle' is the angle between the internal molecular dyad and the **Ox** axis.

Molecule	M1	M2	M3	M4
Symmetry	(x, y, z)	$(x + \frac{1}{2}, -y + \frac{1}{2}, -z)$	$(-x + \frac{1}{2}, y + \frac{1}{2}, -z)$	$(-x, -y, z)$
Angle (°)	45	−45	135	225
M1→ ...	0, 0, 0	$\frac{1}{2}, -2y + \frac{1}{2}, -2z + \frac{1}{4}H_c$	$-2x + \frac{1}{2}, \frac{1}{2}, -2z - \frac{1}{4}H_c$	$-2x, -2y, -\frac{1}{2}H_c$
M2→ ...	$\frac{1}{2}, 2y - \frac{1}{2}, 2z - \frac{1}{4}H_c$	0, 0, 0	$-2x, 2y, -\frac{1}{2}H_c$	$-2x + \frac{1}{2}, \frac{1}{2}, 2z - \frac{3}{4}H_c$
M3→ ...	$2x - \frac{1}{2}, \frac{1}{2}, 2z + \frac{1}{4}H_c$	$2x, -2y, \frac{1}{2}H_c$	0, 0, 0	$\frac{1}{2}, -2y + \frac{1}{2}, 2z - \frac{1}{4}H_c$
M4→ ...	$2x, 2y, \frac{1}{2}H_c$	$2x + \frac{1}{2}, \frac{1}{2}, -2z + \frac{3}{4}H_c$	$\frac{1}{2}, 2y + \frac{1}{2}, -2z + \frac{1}{4}H_c$	0, 0, 0

grams with various search models failed to find the solution. The major reason could be a significant difference of all the trial models from the real structure. Since the Patterson-based analysis is only based on the general molecular features, it was applied in order to obtain complementary information about the structure. It may be mentioned that it was in fact this crystal that was the origin of the approach presented in this manuscript.

Peaks A, B and C in the self-rotation function (Fig. 7*a*) showed the directions of three mutually orthogonal dyads, those of the noncrystallographic symmetry **N**, the internal dyad **D** and their combination **C**, without knowing which peak correspond to which axis.

The map of the Patterson function calculated at a resolution of 3.0 Å showed very strong ripples in the approximate direction $2\mathbf{a} + 2\mathbf{b} - \mathbf{c}$ (Fig. 8*a*). These ripples are at a distance of approximately 3.5 Å and their direction is practically parallel to one of the directions indicated by the self-rotation function (peak A in Fig. 7*a*), with polar angles close to $\varphi = 50°$, $\psi = 120°$. Therefore, we concluded that the direction of the helical axis indicated by the ripples is practically parallel to the noncrystallographic dyad. According to the theory, the presence of two helical molecules linked by a twofold dyad practically parallel to the helical axes should generate an intermolecular peak in the Patterson function.

Indeed, the map at 3.0 Å resolution showed a single strong peak at 4σ (and obviously its enantiomer copy; Fig. 8*b*) with Cartesian coordinates in angstroms of (24.6, 13.7, 13.2). A projection of this vector along the direction of the noncrystallographic axis or helical axis had a length of approximately 16 Å. According to the theory given above (a shift along the twofold axis by approximately 15 Å, half of the period of the molecule), this signified that the two molecules linked by the noncrystallographic dyad were positioned quite naturally side by side. The normal component of the vector for the Patterson peak had a length of 26–27 Å that was compatible with the distance between the centres of the pseudo-parallel molecules.

The choice of direction A in the self-rotation function as the direction of the noncrystallographic axis and the helical axis left one of the directions B and C for the internal molecular dyad normal to the helical axis. Therefore, there were four possibilities for molecular orientation (direct and opposite direction of the dyad along B or C). In space group *P*1, the position of the first molecule can be chosen arbitrarily at the origin of the unit cell and the second molecule was generated following the transformation defined above. This gave four variants of possible model packing (Figs. 9*a*–9*d*). However, rigid-body refinement with *phenix.refine* (Afonine *et al.*, 2005) did not succeed with any of them.

Owing to the difference of approximately 9° between the helical axis and the noncrystallographic dyad, as determined

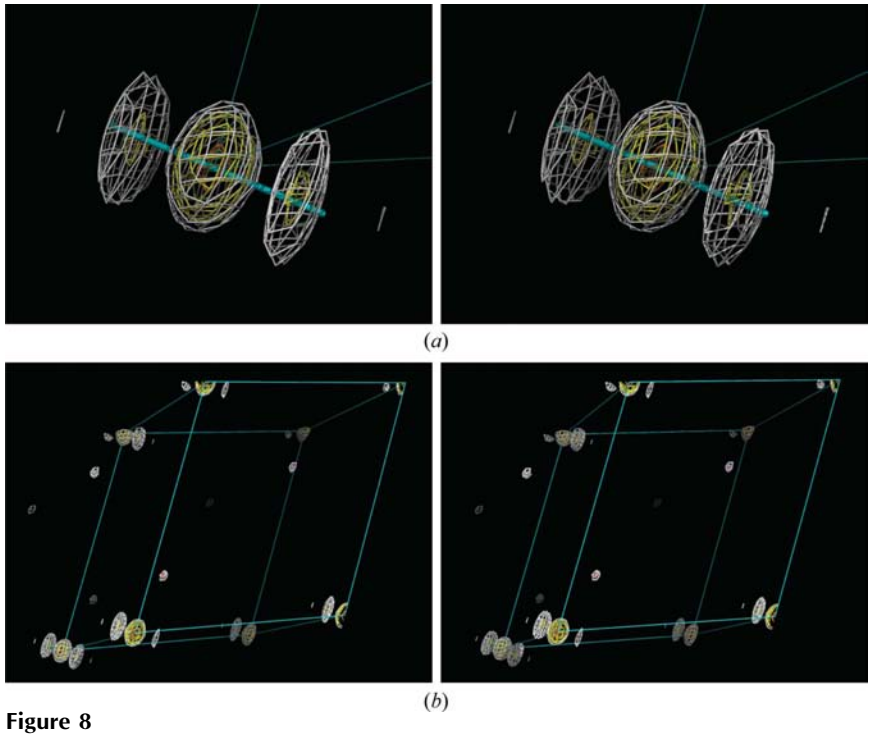

Figure 8
Stereoview of the Patterson function for the *H. sapiens* mitochondrial A site, *P*1 crystal. Map resolution 3 Å; contours are shown at 4σ (white) and 10σ (yellow). (*a*) Peak at the origin and the ripples around; the direction of the noncrystallographic dyad as determined from the self-rotation function is given by a thick cyan line. (*b*) The contents of the unit cell; the off-origin peak and its enantiomer copy are indicated by red and magenta spheres.

above, the direction of the symmetrically generated molecules was less compatible with the Patterson ripples. The strength of the Patterson peak (4σ) and some molecular overlap made us believe that the molecules should be practically parallel. To perform this, the noncrystallographic dyad was assigned to be strictly parallel to the direction of the ripples and four new models were generated. Fig. 9(*e*) shows one of them. These models also removed some molecular overlap that existed in the four previous models. New models had a natural packing of the molecules side by side in layers and 'head to tail' in columns. Two similar models centred at (0, 0, 0) and (2, 2, −1) are nicely aligned and have a distance of approximately 118 Å, thus leaving a space between them for one more molecule rotated by 180° with respect to them.

By combining this information, we were sure that the packing found corresponds to the solution of the crystal. Nevertheless, none of these four new models refined to reasonable values of the *R* factor. Since it was only the first practical example of the application of this approach, we did not pursue larger modifications of the model obtained with further refinement.

Subsequently, the structure of the *P*1 crystal of the *H. sapiens* mitochondrial A site was solved independently (Kondo & Westhof, 2008). Comparison of the result (Fig. 9*f*) with the solution predicted by the Patterson-based analysis (Fig. 9*e*) showed their nice coincidence (Fig. 10*a*). The impossibility of decreasing the *R* factors was not caused by a wrong position of the model but by the difference between the search model and the correct structure (the root-mean-square deviation between the search model and one of the two duplexes in an asymmetric unit of the correct structure is 6.7 Å for the corresponding atoms of the phosphate-ribose backbone). This also explained the failure of standard molecular replacement.

To check the compatibility of the Patterson peak with the solution, the final model was shifted by this Patterson vector. Fig. 10(*b*) shows a superposition of the final and shifted models. Indeed, one of the dimers (on the left in the image) being shifted superposes well in its major part with the second dimer (on the right in the image) oriented differently. A shift by a half of the period along the model is necessary to obtain such a superposition.

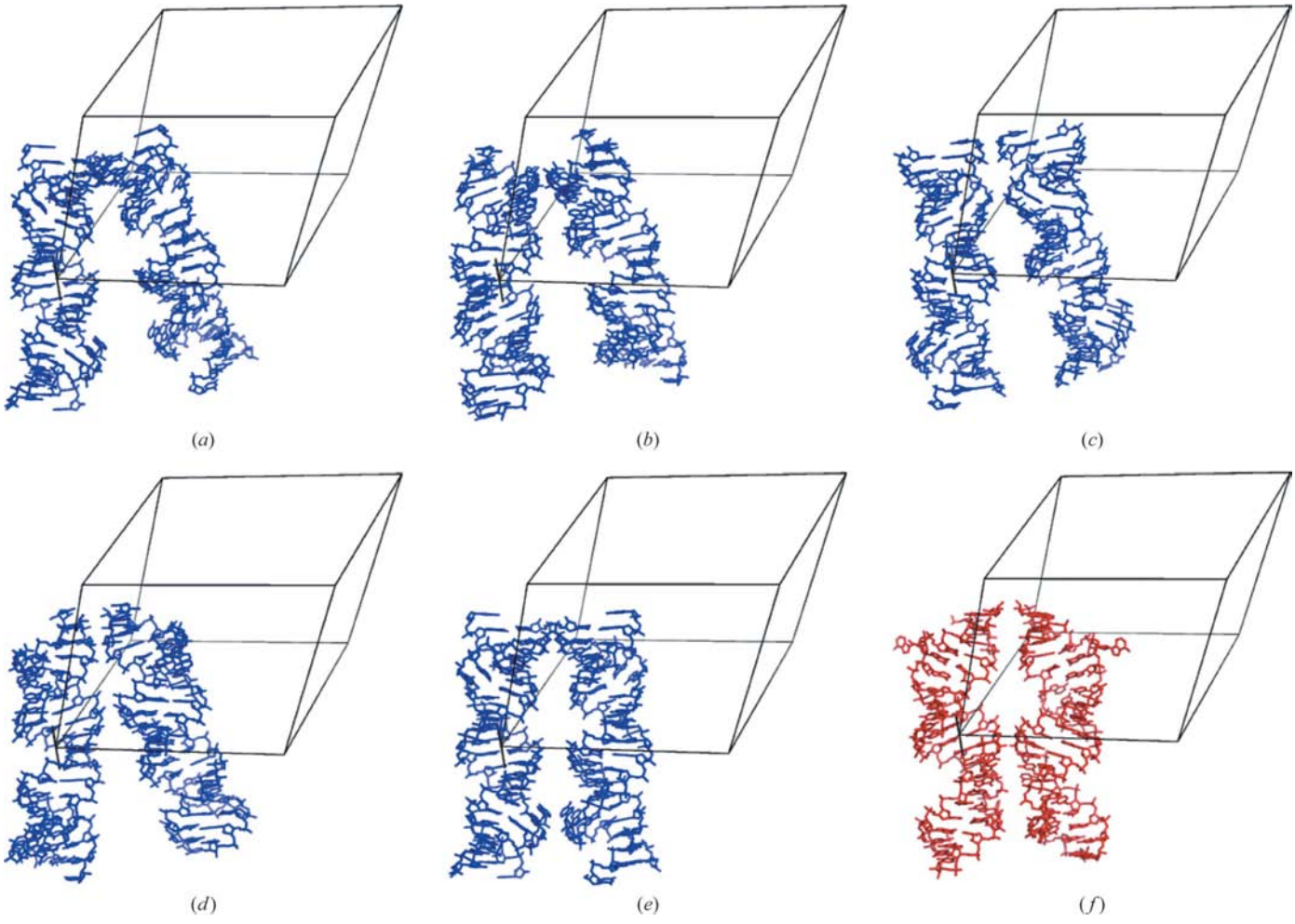

Figure 9
Packing of two model dimers of the *H. sapiens* mitochondrial A site in a *P*1 crystal. (*a*–*d*) Four possible solutions suggested by the Patterson analysis with the originally determined directions of the noncrystallographic axis and helical axis. (*e*) Packing after alignment of the axes. (*f*) The final model.

In summary, for this crystal the Patterson-based search successfully indicated the molecular orientation and position without running a molecular-replacement procedure and the use of a particular model.

6. Structure solution of the *H. sapiens* mitochondrial A site, $P2_12_12_1$ crystal

The crystal of the mitochondrial A site belongs to space group $P2_12_12_1$, with unit-cell parameters a = 33.56, b = 39.22, c = 120.85 Å. The asymmetric unit contains one duplex, with the dyad perpendicular to the helical axis. The molecular-replacement method using the program *AMoRe* (Navaza, 1994) with various search models failed to find the solution.

By its anisotropy, the central peak of the Patterson map at 3 Å resolution indicated that the helical axis is practically parallel to the **Oz** axis; two peaks are clearly observed at distances of 3.5 and 30 Å. The self-rotation function showed the direction of the internal dyad to be more or less parallel to the crystallographic axis (1, 0, 0) or (0, 1, 0) (the angle φ, the axis with **Ox**, is approximately 0° or 90°). The Patterson analysis for both these possible model orientations, applied in the manner discussed above, led us to the model centre at position (0.84, 0.03, 0.76) for φ = 0° and to no solution for φ = 90°.

The atomic parameters of the model of the A site positioned accordingly were refined with the program *CNS* (Brünger *et al.*, 1998) through a combination of rigid-body refinement, simulated annealing, crystallographic conjugate-gradient minimization refinement and *B*-factor refinement. The final R factor was 24.8% for data in the resolution range 100–2.5 Å ($R_{\rm free}$ = 26.6% for 10% of the observed data). The detailed crystal structure (Fig. 11) will be discussed elsewhere (Kondo & Westhof, in preparation).

7. Conclusions

Analysis of the details of the Patterson functions for molecules with helical symmetry illustrates how this information may be used to determine the structure. This 'Patterson assistance' may be especially important in molecular replacement when the search model is poor, when neither the routine procedure of cross-rotation and translation searches nor the six-dimensional search give an obvious answer owing to this model imperfection and when only the experimental structure-factor magnitudes may be used as certain information. Knowledge of the space group and general symmetry features of the molecule can provide a guide to molecular position and thus simplify structure solution. The Patterson functions and their auxiliary peaks, which are usually ignored for structure analysis, can be used as such a tool. This article illustrates the application of such an approach to previously determined structures and to difficult cases of the structure solution of RNA duplexes containing the *H. sapiens* cytoplasmic or mitochondrial A site. Appendix *A* shows the limits of the method in terms of similarity of the directions of the axes, the internal helical axis and of the crystallographic rotation. Similarly, decreasing of the helical symmetry of the molecule itself, for example by the binding of other molecules to RNA, makes the density of the original molecule more different from that of its symmetrically

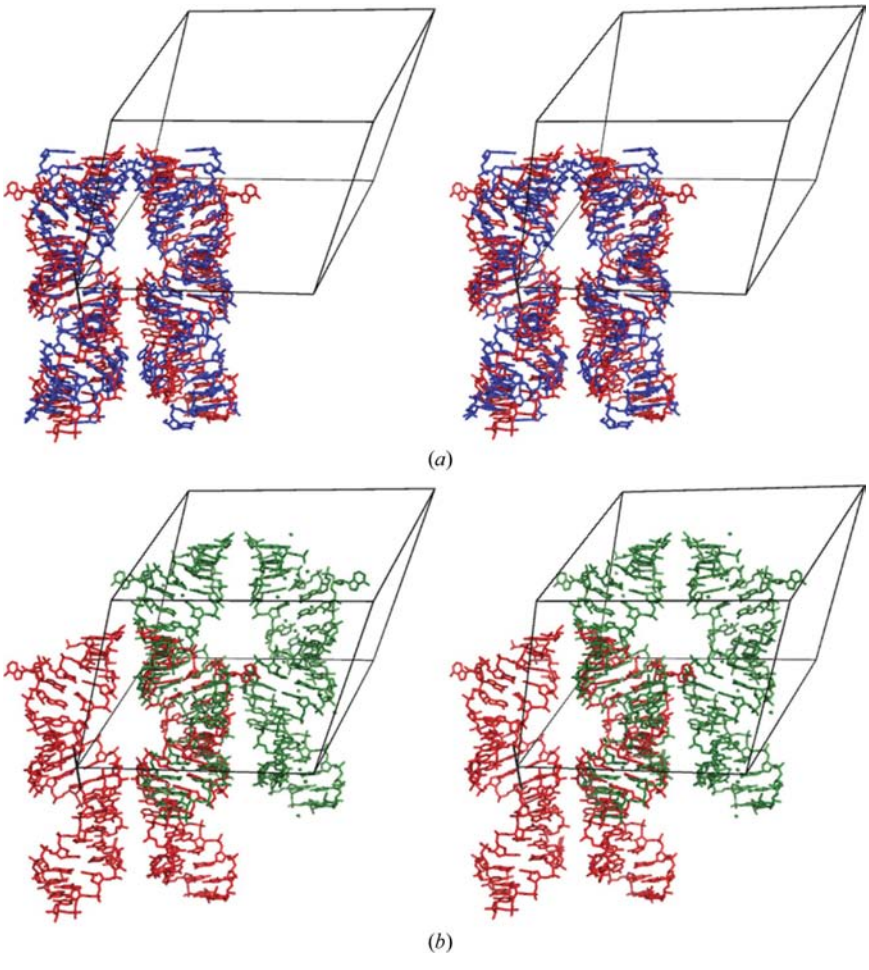

Figure 10
Stereoview of the packing of two molecules of the *H. sapiens* mitochondrial A site in a *P*1 crystal. (*a*) The solution (red) and the model obtained by the Patterson-based analysis (blue); a significant difference between the correct structure and the search model, especially at their ends, was responsible for the failure of molecular replacement. (*b*) The solution (red) and its copy (green) shifted accordingly to the peak in the Patterson map; note the overlap between the two molecules oriented in opposite directions.

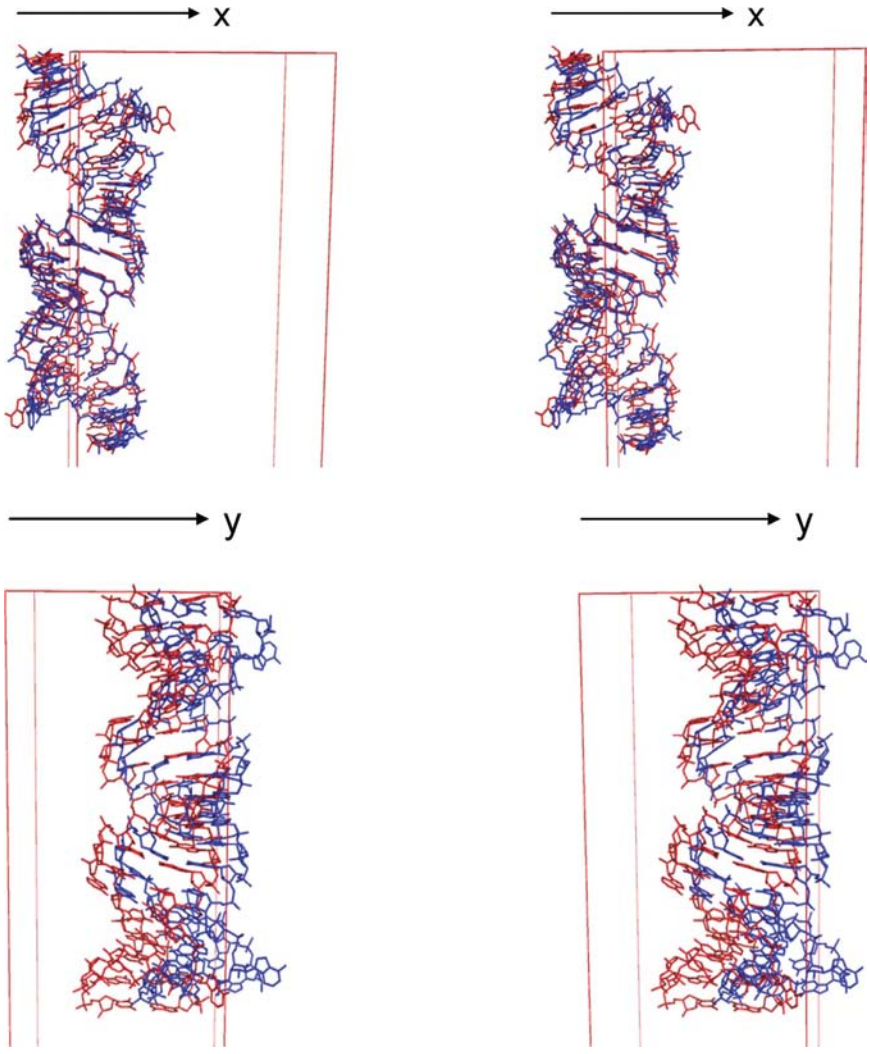

Figure 11
Stereoview of the superimposition between the initial model solved by the *ab initio* analysis (blue) and the final refined structure (red). Two orthogonal views are shown.

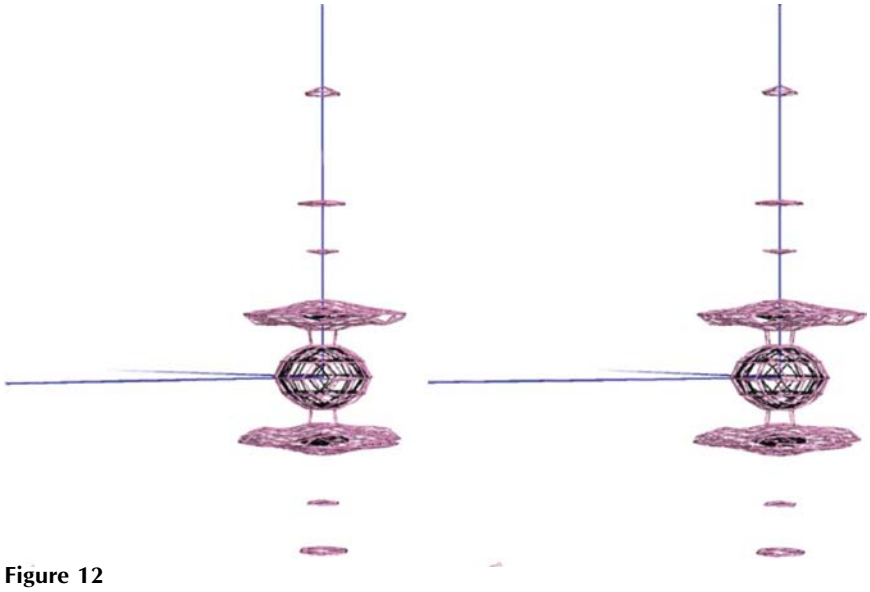

Figure 12
Stereoview of the Patterson function for the *H. sapiens* mitochondrial A site, trigonal crystal. Map resolution 3 Å; contours are shown at 4σ (pink) and 10σ (black); **Ow** is vertical. The distance from the centre of the first ripple to the origin is approximately 3.5 Å.

related copy after translation and makes the method inefficient. However, a few bumped-out nucleotides or small antibiotics bound to an RNA duplex leave the Patterson out-of-origin peaks sufficiently strong for this type of analysis, as demonstrated with the mitochondrial A site crystals.

APPENDIX *A*
H. sapiens mitochondrial A site, trigonal crystal

A1. Data description

A further crystal of the *H. sapiens* mitochondrial A site belonged to space group $P3_121$ (or $P3_221$), with unit-cell parameters $a = b = 66.35$, $c = 57.35$ Å and one duplex per asymmetric unit. A self-rotation function for the trigonal crystal (Fig. 7*b*) showed two possibilities for the internal molecular dyad, either parallel to the crystallographic threefold axis or normal (approximately $\varphi \simeq 30^\circ$ from the axis **Ox**), both of which were compatible with the size of the unit cell and both of which were considered at the initial stages. The origin peak of the Patterson map showed ripples in the **Ow** direction (Fig. 12). However, the ripples were expanding around this axis and it could be seen that each of the two largest blobs was composed from six smaller ones at its periphery that were merged together. This means that the angle between the molecular helical axis and **Oz** is as large as 20–25° and the current method might not be applicable to this data set. Nevertheless, we tried it in the absence of other possibilities at the time.

A2. Self-rotation function and Patterson analysis

Once the direction of the helical axis had been identified as being roughly parallel to **Oz**, the internal molecular dyad could only be in the plane *xOy*. The self-rotation function showed peaks corresponding to noncrystallographic twofold symmetry in this plane. In fact, in maps with optimal conditions it could be observed that the peak at $\varphi \simeq 30^\circ$ (the angle between the dyad and the **Ox** axis) was split into two close peaks (Fig. 7*b*). According to the space-group symmetries, this would mean the presence of two triads of molecules, one with a dyad along $\varphi \simeq 25$, 145, 265 (or 205, 325, 85°) and the second with a dyad along $\varphi \simeq -25$, 95, 215° (or 155, 275 and 35°).

Table 2
Parameters of the six symmetry-related molecules for the trigonal crystal of the *H. sapiens* mitochondrial A site.

'Angle' is the angle between the internal molecular dyad (in the plane xOy) and the **Ox** axis.

Molecule	M1	M2	M3	M4	M5	M6
Angle (°)	φ	$\varphi + 120$	$\varphi + 240$	$120 - \varphi$	$-\varphi$	$240 - \varphi$
Value	25	145	265	95	−25	215
$P3_121$	x, y, z	$-y, x-y, z+1/3$	$-x+y, -x, z+2/3$	$y, x, -z$	$x-y, -y, -z+2/3$	$-x, -x+y, -z+1/3$
$P3_221$	x, y, z	$-y, x-y, z+2/3$	$-x+y, -x, z+1/3$	$y, x, -z$	$x-y, -y, -z+1/3$	$-x, -x+y, -z+2/3$

Table 2 gives the centres of symmetry-linked molecules in both possible space groups where $0 \leq (x, y, z) < 1$ represent the coordinates of the centre of the molecule M1 with the dyad along $\varphi \simeq 25^\circ$ (205°).

It follows from Table 2 that the coordinates (u, v) of these peaks should be the same for both possible space groups, $P3_121$ or $P3_221$, while the w coordinate is dependent on the space group. Analysis of the Patterson maps suggested that $P3_121$ was the correct choice.

The Patterson peaks for the smallest rotation, 50°, were analyzed in the manner discussed in previous sections. This reduced the number of possible molecular positions to only four, including (0.53, 0.79, 0.22). We failed to resolve the ambiguity by interpreting lower peaks (below 3σ) of the Patterson function. Model refinement for all four possible positions also did not allow us discriminate the solution.

A3. Choice of space group

Owing to the expected significant deviation of the molecular helical axis from the threefold axis **Oz**, it was not guaranteed that the molecules linked by the threefold axis (M1→M2, M2→M3, M3→M1, M4→M6, M6→M5, M5→M4) would generate Patterson peaks. However, if this were the case then it follows from Table 2 that the coordinates (u, v) of these peaks should be the same for both possible space groups, $P3_121$ or $P3_221$,

$$(-x-y, x-2y), (-x+2y, -2x+y), (2x-y, x+y),$$
$$(-x-y, -2x+y), (2x-y, x-2y), (-x+2y, x+y). \quad (8)$$

At the same time, the w coordinate should be common to all six peaks and very different for the two space groups: $1/3 - (H/3c)$ for $P3_121$ and $2/3 - (H/3c)$ for $P3_221$. For $H \simeq 30$ Å and $c = 57.35$ Å, this gave values of $1/3 - (H/3c) \simeq 0.158$ and $2/3 - (H/3c) \simeq 0.492$.

Of the Patterson maps at 3, 6 and 9 Å resolution, only the last one showed a sextet of peaks with the same w coordinate at 3σ. Its value $w_{\rm sext}$ was equal to 0.13 and thus suggested space group $P3_121$ as the correct choice.

A4. Positional search

Let $(u_{\rm sext}, v_{\rm sext})$ represent the coordinates of different peaks of the sextet described in the previous section, including those translated by the crystal period. The system of equations

$$-x - y = u_{\rm sext}, \quad x - 2y = v_{\rm sext} \quad (9)$$

for the coordinates (x, y, z) of the molecule M1 had 18 solutions in the range (0, 1) with no information about the z coordinate.

To resolve the ambiguity and to find the z coordinate, extra information was required. According to §2, for helical molecules with pseudo-parallel axes the strongest signal in the Patterson maps should correspond to the molecules with smallest rotation angle between them. For the supposed packing, it would be the molecules M5→M1 (rotation by approximately 50°) and symmetry-related pairs. In space group $P3_121$ the coordinates of the peak should be

$$(u_{51}, v_{51}, w_{51}) = \left(y, 2y, 2z - \frac{2}{3} - \frac{50}{360}\frac{H}{c}\right). \quad (10)$$

In addition to the analyzed sextet, the Patterson maps at 6 and 9 Å resolution contained a single independent peak above 3σ. Two of its symmetry-related copies had coordinates compatible with the condition $v = 2u$, giving $(y, z) = (0.75, 0.22)$ or $(0.25, 0.01)$. This reduced the number of solutions to only four, including that of (0.53, 0.79, 0.22). We tried to resolve the ambiguity by interpreting lower peaks (below 3σ) of the Patterson function in terms of intermolecular vectors, for example for M1→M4. All these attempts led to values that were incompatible with the previous ones and we failed to extract the correct solution by this method as would be expected for highly nonparallel models.

A5. Comparison with the solved structure

The atomic structure of the crystal was subsequently solved by conventional molecular replacement using a new available model (Kondo & Westhof, 2008). The final solution had a dyad in the plane xOy making an angle of 25° with **Ox**. The helical axis of the model made an angle of roughly 25° with **Oz**. The coordinates of the molecular centre were (0.569, 0.756, 0.415), where the x and y values corresponded well to the values found theoretically. Therefore, even when the helical axis of the molecule and the rotation axis were significantly nonparallel, beyond the expected limits for application of the Patterson-based analysis, some characteristics of the solution were predicted, with the only (but a significant) error in the z coordinate.

During part of this work, JK was supported by the Japan Society for the Promotion of Science. We are grateful to E. Westhof and D. Moras for helpful discussions, suggestions and support of the project. The constructive criticism of the referees is much appreciated. We also thank A. McEwen for his help in preparation of the manuscript.

References

Afonine, P. V., Grosse-Kunstleve, R. W. & Adams, P. D. (2005). *CCP4 Newsl.* **42**, contribution 8.

Brünger, A. T., Adams, P. D., Clore, G. M., DeLano, W. L., Gros, P., Grosse-Kunstleve, R. W., Jiang, J.-S., Kuszewski, J., Nilges, M., Pannu, N. S., Read, R. J., Rice, L. M., Simonson, T. & Warren, G. L. (1998). *Acta Cryst.* D**54**, 905–921.
DeLano, W. L. (2002). *The PyMOL Molecular Graphics System.* DeLano Scientific, San Carlos, USA. http://www.pymol.org.
Feynman, R. & Leighton, R. (1985). *Surely You're Joking, Mr Feynman!* New York & London: W. W. Norton.
Franklin, R. E. & Gosling, R. G. (1955). *Acta Cryst.* **8**, 151–156.
Harker, D. (1936). *J. Chem. Phys.* **4**, 381–390.
Kim, S.-H. & Rich, A. (1969). *Science*, **166**, 1621–1624.
Kondo, J., Urzhumtsev, A. & Westhof, E. (2006). *Nucleic Acids Res.* **34**, 676–685.
Kondo, J. & Westhof, E. (2008). *Nucleic Acids Res.* **36**, 2654–2666.
McCoy, A. J., Grosse-Kunstleve, R. W., Storoni, L. C. & Read, R. J. (2005). *Acta Cryst.* D**61**, 458–464.
Magdoff, B. S., Crick, F. H. C. & Luzzati, V. (1956). *Acta Cryst.* **9**, 156–162.
Navaza, J. (1994). *Acta Cryst.* A**50**, 157–163.
Ogihara, N. L., Weiss, M. S., Degrado, W. F. & Eisenberg, D. (1997). *Protein Sci.* **6**, 80–88.
Pan, B., Mitra, S. N. & Sundaralingam, M. (1998). *J. Mol. Biol.* **283**, 977–984.
Patterson, A. L. (1934). *Phys. Rev.* **46**, 372–376.
Patterson, A. L. (1935). *Z. Kristallogr.* **90**, 517–542.
Rossmann, M. G. & Arnold, E. (2001). Editors. *International Tables for Crystallography*, Vol. F, pp. 263–292. Dordrecht: Kluwer Academic Publishers.
Sakurai, T., Rao, S. T., Rubin, J. & Sundaralingam, M. (1971). *Science*, **172**, 1234–1237.
Tong, L. & Rossmann, M. G. (1990). *Acta Cryst.* A**46**, 783–792.
Tong, L. & Rossmann, M. G. (1997). *Methods Enzymol.* **276**, 594–611.
Urzhumtsev, A. & Urzhumtseva, L. (2002). *J. Appl. Cryst.* **35**, 750.
Urzhumtseva, L. M. & Urzhumtsev, A. G. (1997). *J. Appl. Cryst.* **30**, 402–410.
Urzhumtseva, L. M. & Urzhumtsev, A. G. (2008). *J. Appl. Cryst.* **41**, 479–480.
Vernoslova, E. A. & Lunin, V. Yu. (1993). *J. Appl. Cryst.* **26**, 291–294.